International Journal of Plasticity 59 (2014) 84–107

Contents lists available at ScienceDirect

International Journal of Plasticity

journal homepage: www.elsevier.com/locate/ijplas

Measurement of the Bauschinger behavior of sheet metals by three-point bending springback test with pre-strained strips

Shun-lai Zang [a,*], Myoung-Gyu Lee [b], Li Sun [c], Ji Hoon Kim [d]

[a] School of Mechanical Engineering, Xi'an Jiaotong University, No. 28, Xianning Road, Xi'an, Shaanxi, China
[b] Graduate Institute of Ferrous Technology, Pohang University of Science and Technology, San 31, Hyoja-dong, Nam-gu, Pohang, Geongbuk 790-784, Republic of Korea
[c] Manufacturing Process Research, General Motors China Science Lab, GM (China) Investment Co., Ltd., No. 56, Jinwan Road, Shanghai, China
[d] School of Mechanical Engineering, Pusan National University, 2 Busandaehak-ro 63beon-gil, Geumjeong-gu, Busan 609-735, Republic of Korea

ARTICLE INFO

Article history:
Received 17 October 2013
Received in final revised form 20 February 2014
Available online 5 April 2014

Keywords:
Bauschinger effect
Constitutive model
Parameter identification
Pre-strain effect
Three-point bending

ABSTRACT

In this paper, a novel approach is proposed to measure the Bauschinger effect, transient behavior and permanent softening of metallic sheet subjected to reverse loading. The hardening parameters related to the Bauschinger effect, transient behavior and permanent softening are optimized from the springback profiles of three-point bending tests with pre-strained sheets. Taking the dual phase steel sheet DP780 as an example, its Bauschinger effect, transient behavior and permanent softening determined from the new approach are compared with those of the cyclic simple shear method. Finite element simulations are also performed for three-point bending and U-draw/bending of base (as-received) and pre-strained DP780 steel sheets to validate the suggested approach. The results show that the aforementioned hardening behavior determined from the new approach shows good agreements with those of cyclic simple shear tests. Moreover, reasonable springback predictions for three-point bending and U-draw/bending tests are obtained as well. In particular, the proposed approach is quite suitable for the industrial applications because only uni-axial tension and three-point bending tests are required.

1. Introduction

In sheet metal forming, springback is more pronounced with the increasing applications of the material that has higher strength. For example, the recent advanced high strength steels (AHSS) produce larger springback than the conventional steels. To compensate the springback, considerable efforts have been made to predict it accurately by finite element method. Due to the benefit of time cost, the classical elastic–plastic constitutive models are still frequently used in the numerical simulations of springback (Wagoner et al., 2013).

Within the phenomenological model, hardening behavior, such as the Bauschinger effect, transient behavior and permanent softening (see Fig. 1), is described by the evolution of internal variables with plastic strain (Chaboche, 1986, 2008). For simplicity, the Bauschinger effect, transient behavior and permanent softening are termed as the Bauschinger behavior in the present work. The isotropic hardening model has been recognized well that it over-estimates the flow stress under strain path reversal by missing the Bauschinger behavior, while the pure kinematic hardening law under-estimates it

* Corresponding author. Tel.: +86 29 82668607x806; fax: +86 29 82664360.
E-mail address: shawn@mail.xjtu.edu.cn (S.-l. Zang).

http://dx.doi.org/10.1016/j.ijplas.2014.03.015
0749-6419/

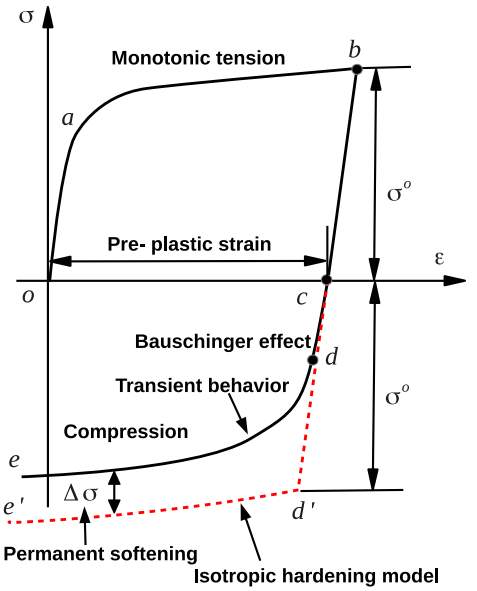

Fig. 1. A schematic unloading curve under reverse loading to illustrate the Bauschinger effect, transient behavior and permanent softening. Here curve *oabcde* represents the experimental flow stress during uni-axial tension–compression, curve *oabcd′e′* is predicted from the isotropic hardening model without these hardening behavior.

(e.g. Lee et al., 2005a, 2007; Zhang et al., 2007; Lee et al., 2012b). In order to predict accurately the Bauschinger behavior, the combination of isotropic and non-linear kinematic hardening is usually employed (e.g. Yoshida and Uemori, 2002; Chung et al., 2005; Haddadi et al., 2006; Zang et al., 2011a).

As already known, the cyclic mechanical behavior of metallic sheet is required to calibrate the material parameters of aforementioned combined isotropic-kinematic hardening model (Yoshida et al., 2002; Boger et al., 2005; Bouvier et al., 2006). Therefore the development of experimental device and method is an important work in order to measure the cyclic mechanical behavior of metallic sheet. There are several experimental devices which can measure this cyclic mechanical behavior of sheet metal mainly to measure the Bauschinger behavior. Often, these experiments can be classified into three main categories: (i) in-plane tension–compression test; (ii) in-plane cyclic simple shear test; (iii) bending-reverse bending test.

For the in-plane tension–compression test, the aim is to measure the hardening behavior of metallic sheet under reversed uni-axial loading. However, the compressive strain range attainable with this kind of test is severely limited due to the buckling. To prevent the buckling in thickness direction, two solid plates are usually placed along the sides of the sheet specimen and then clamping force is applied on each plate (e.g. Yoshida et al., 2002; Boger et al., 2005; Lee et al., 2005b; Kuwabara, 2007; Cao et al., 2009; Sun and Wagoner, 2011; Verma et al., 2011; Andar et al., 2012; Piao et al., 2012; Sun and Wagoner, 2013). The introduced solid plate and applied clamping force result in the friction and bi-axial effect during compression. Therefore the corrections of friction and bi-axial effect are required for this in-plane tension–compression test (Lee et al., 2005b). By optimizing specimen geometry and clamping force, larger compressive strain has been reported (Boger et al., 2005; Piao et al., 2012). For small thickness sheet, the approach that several pieces of the sheet are adhesively bonded together before machining has also been employed to prevent the buckling (Yoshida et al., 2002). Usually, there is an unsupported gap between grip of material test system and solid plates, which leads to the so-called L-buckling (Boger et al., 2005). To suppress the L-buckling, a new fixture has been developed with four-block wedge design. The design allows blocks to freely move in the uni-axial loading direction while providing the clamping force in the thickness direction for the entire length of the specimen (Cao et al., 2009). Although the in-plane tension–compression test is suitable to understand the plastic behavior of metallic sheet along reversal strain path, the buckling problem, the correction of friction, bi-axial effect and misalignment severely limit its industrial applications. Moreover, it is hard to determine if a small buckling happened during compression by naked eyes due to side plates.

To achieve a large strain under reverse loading, the in-plane cyclic simple shear test was successfully developed (Hu et al., 1992) and received an increasing attention during the past decade (e.g. Yoon et al., 2005; Bouvier et al., 2006; Thuillier and Manach, 2009; Lee et al., 2012a; Yin et al., 2012; Zang et al., 2013b). In the simple shear test, a rectangular gauge area is deformed to parallelogram along the length direction while the width is fixed. Obviously, the strain field in the deforming zone of simple shear specimen is complicated. To formulate the deformation of simple shear, the shear component of an averaged deformation gradient in rectangular gauge area is usually adopted. Thanks to the digital image correlation system, the three-dimensional displacement field in the deformation region can be obtained, and then the deformation gradient field

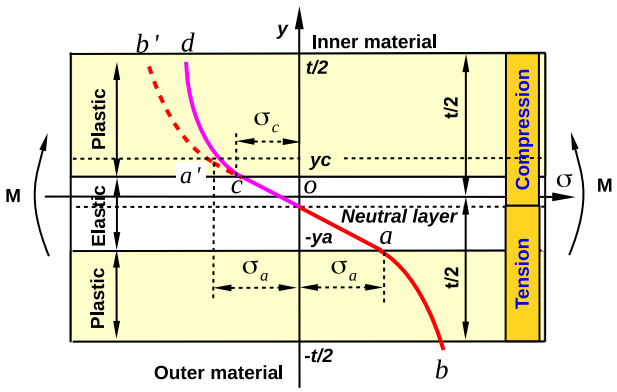

(a) Stress spatial distribution during bending for a pre-strained sheet.

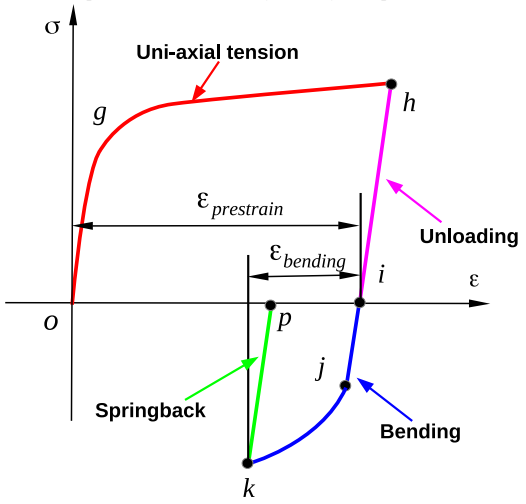

(b)Stress time-like evolution for the inner material.

Fig. 2. A schematic (a) stress distribution during the bending for a pre-strained sheet, where the curve $oa'b'$ stands for the compressive stress distribution for an imagined material which has no Bauschinger behavior, the curve *dcoab* represents the real material. (b) the stress evolution for the inner material during the pre-strain, unloading, three-point bending and springback.

is calculated (Tang et al., 2010; Yin et al., 2012; Zang et al., 2013b). However, the in-plane cyclic simple shear test has also several disadvantages as already pointed by previous researchers. Firstly, the deformation may be non-homogeneous throughout the simple shear gauge area (Bouvier et al., 2006). Secondly, the stress state in simple shear test is complicated. It results in the fact that the planar anisotropy has an influence on the measured shear stress of cyclic simple shear test (Thuillier and Manach, 2009; Zang et al., 2013b). Although the aforementioned disadvantages, the simplicity of the specimen geometry, the absence of localization and the large plastic deformation still make the simple shear test attractive.

As for the bending-reverse bending test, the reason why the Bauschinger behavior can be determined from this test lies in that the inner/outer materials experience compression-tension/tension–compression in bending-reverse bending procedure. Therefore the punch load or bending moment absolutely depends on the cyclic mechanical behavior of metallic sheet. Starting from Yoshida's work (Yoshida et al., 1998), the approach that the cyclic stress–strain responses are determined from a cyclic bending experiment by using an inverse method has gained some popularity (e.g. Geng et al., 2002; Yoshida et al., 2003; Carbonnire et al., 2009; Eggertsen and Mattiasson, 2009). Comparing with the in-plane tension–compression test, the bending-reverse bending test cannot provide the knowledge on the hardening behavior of material under one-dimensional loading. Hence this test seems not suitable to investigate the unknown cyclic mechanical behavior for a new metallic sheet.

In this work, a novel approach is developed in order to simply estimate the Bauschinger behavior. For a pre-strained sheet, the inner material experiences tension–compression deformation after the subsequent three-point bending. Therefore the Bauschinger behavior has an influence on the bending moment before springback. Since the springback is mainly related to the elastic properties of the material and the bending moment before unloading, the Bauschinger behavior of metallic sheet can be determined from the springback of three-point bending test with pre-strained sheet. Comparing with the existing techniques, the suggested approach only involves the uni-axial tension with/without unloading and three-point bending test. These tests are easily available with the help of the common material test system and not required for complicated

strain measurement devices. Thus the new approach seems quite suitable for the industrial applications. In Section 2, the bending moment for a pre-strained sheet is analysed, meanwhile the constitutive model used in this work is briefly summarized. In Section 3, the experimental works are described and the strategy of material parameters identification is discussed in Section 4. In material parameters identification, the springback profile of three-point bending test is simulated by the finite element method, the finite element models are described in Section 5. Finally, in Section 6 the material parameters calibrated from the new approach are compared with those of simple shear test, and then applied to springback problems of three-point bending and U-draw/bending to confirm its validity.

2. Theoretical background

In this section, the reason why we can determine the Bauschinger behavior from three-point bending springback with pre-strained sheet is explained. The theoretical background for the new method is described. Meanwhile the constitutive model used in this work is briefly summarized.

2.1. Three-point bending for pre-strained strip

For one-dimensional loading, the magnitude of elastic recovery is proportional to the flow stress before unloading and inversely proportional to Young's modulus (Sun and Wagoner, 2011). In case of a three-dimensional problem, the final springback profile depends on the bending moment before unloading and elastic properties of the material. Generally speaking, the larger the magnitude of bending moment, the larger the amount of springback becomes for a certain material. Moreover, it can be claimed that there is a unique relationship between bending moment and springback (Lee et al., 2005a). This means that the bending moment before unloading can be uniquely determined by the magnitude of springback if the Young's modulus has been captured well. Therefore, in essence, the identification strategy optimizing material parameters from the final springback profile of three-point bending test is identical to the method determining the aforementioned hardening behavior from the bending moment.

For a pre-strained sheet, the material has stretched to a prescribed engineering strain. During the subsequent three-point bending, the outer material experiences continuous tangential tensile deformation, while the inner material is compressed along the tangential direction. Fig. 2(a) is a schematic illustration on the stress distribution along thickness direction during the bending for a pre-strained sheet. Its deformation history can be divided into four procedures, i.e. uni-axial tension, unloading, three-point bending and final springback. There are two regions in Fig. 2(a), i.e. tension and compression, which are separated by the neutral layer. For any elastic–plastic material, the bending will make the material near the neutral layer lies in the elastic zone, while the elastic–plastic deformation occurs in the other material. Due to the existence of the Bauschinger effect, the re-yielding stress in the compression region is lower than that of tension region, i.e. $|\sigma_c| < |\sigma_a|$ as depicted in Fig. 2(a). Note that, after initial tension is all released, for the subsequent pure bending, the neutral layer is not the central layer any more since the hardening data is not symmetric with respect to the central layer. Then the moment per unit width in three-point bending for a pre-strained sheet can be written as

$$M = \int_{-t/2}^{-ya} \sigma_{tension} \cdot y \cdot dy + \int_{-ya}^{yc} \sigma_{elastic} \cdot y \cdot dy + \int_{yc}^{t/2} \sigma_{compression} \cdot y \cdot dy \tag{1}$$

where $\sigma_{tension}$ stands for the tangential stress in the tension region, $\sigma_{compression}$ represents the stress state in compression region, $\sigma_{elastic}$ is the elastic stress near neutral layer, t is the thickness of a pre-strained sheet, ya and yc are the distances of elastic zones to neutral layer in tension and compression regions, respectively.

The last term in the right side of Eq. (1) indicates that the bending moment for a pre-strained sheet is significantly influenced by the Bauschinger behavior. To understand it well, we can analyze the tangential stress evolution for the inner material during three-point bending for a pre-strained sheet. Fig. 2(b) is the stress evolution for the inner material in the whole deformation history, i.e. uni-axial tension, unloading, three-point bending and final springback. Here $\varepsilon_{prestrain}$ depends on the prescribed engineering strain in the uni-axial tension, while the magnitude of bending strain $\varepsilon_{bending}$ can be calculated from

$$\varepsilon_{bending} = \frac{t}{2r} \tag{2}$$

where r is the bending radius, t is the thickness of metallic sheet.

By changing $\varepsilon_{prestrain}$ and $\varepsilon_{bending}$, the final springback profile of three-point bending test indirectly reflects the cyclic mechanical behavior under reverse loading. Then the Bauschinger behavior can be determined from these final springback profiles of three-point bending tests with pre-strained sheets. Comparing with the bending-reverse bending method, the new approach has several advantages. Firstly, the pre-strain can be prescribed randomly with a wide range of plastic strain. Meanwhile the magnitude of bending strain is possible to reach a large value because we do not need to reversely bend the specimen.

2.2. Constitutive model

In the present work, a combined isotropic-kinematic hardening model was used to capture the hardening behavior (Chun et al., 2002; Zang et al., 2011a). The global strain hardening is described by an isotropic hardening rule. A two-term kinematic hardening model was adopted to consider the hardening behavior under strain path reversal. The constitutive equations were derived by applying the associated flow rule and hypo-elastic assumption, which are summarized in the following paragraphs. For convenience, the used constitutive model was termed as the ANK (anisotropic non-linear kinematic) model following the convention of the work by Chun et al. (2002). For more details, the constitutive model can be found in the work by Zang et al. (2011a). In addition, it is worth noting that all material hardening parameters are constants in this work.

For a combined isotropic-kinematic hardening model, the yield criterion F is defined as

$$F = f(\boldsymbol{\sigma} - \boldsymbol{\alpha}) - \bar{\sigma}(\bar{\varepsilon}^p) = 0 \tag{3}$$

where f is the first order homogeneous yield function, $\boldsymbol{\sigma}$ is the Cauchy stress tensor and $\boldsymbol{\alpha}$ is the back-stress tensor, $\bar{\varepsilon}^p$ is the equivalent plastic strain, $\bar{\sigma}(\bar{\varepsilon}^p)$ is the equivalent stress which is used to measure the size of the current yield surface as a first order homogeneous function of equivalent plastic strain.

For the two-term kinematic hardening model, the evolution equation of back-stress can be written as

$$\dot{\boldsymbol{\alpha}} = \dot{\boldsymbol{\alpha}}_1 + \dot{\boldsymbol{\alpha}}_2 \tag{4}$$

where $\dot{\boldsymbol{\alpha}}_1$ is the evolution equation for a non-linear Chaboche kinematic hardening model (Chaboche, 1986), $\dot{\boldsymbol{\alpha}}_2$ is the evolution equation for a linear Ziegler model (Ziegler, 1959). These equations can be defined as

$$\dot{\boldsymbol{\alpha}}_1 = \frac{C_1}{\bar{\sigma}}(\boldsymbol{\sigma} - \boldsymbol{\alpha})\dot{\bar{\varepsilon}}^p - \gamma_1 \boldsymbol{\alpha}_1 \dot{\bar{\varepsilon}}^p \tag{5a}$$

$$\dot{\boldsymbol{\alpha}}_2 = \frac{C_2}{\bar{\sigma}}(\boldsymbol{\sigma} - \boldsymbol{\alpha})\dot{\bar{\varepsilon}}^p \tag{5b}$$

where C_1, γ_1 and C_2 are material hardening parameters.

As for isotropic hardening model, a modified isotropic hardening model was used for $\bar{\sigma}(\bar{\varepsilon}^p)$ to predict a relative flat stress–strain curve (Zang et al., 2011a),

$$\bar{\sigma}(\bar{\varepsilon}^p) = \sigma_\circ + R_{ih} = \sigma_\circ + Q(1 - e^{-b\bar{\varepsilon}^p}) - \frac{C_1}{\gamma_1}(1 - e^{-\gamma_1 \bar{\varepsilon}^p}) \tag{6}$$

where $\sigma_\circ$ represents the initial yield stress, R_{ih} is the isotropic hardening. C_1 and γ_1 are the same as the parameters in Eq. (5a). Q and b are material hardening parameters.

Finally, it is worth noting that the consistency condition should be satisfied for any combined isotropic-kinematic hardening model (Chung and Park, 2013). Since the present ANK model is the Ziegler type-based kinematic hardening model with associated flow rule and plastic work equivalence principle, the consistency condition is confirmed.

3. Experiments

A dual phase steel designated by DP780 with a nominal thickness of 1.30 mm was considered in the present work. The as-received material is not performed for any post-processing treatment, and its chemical composition is listed in Table 1. In the following subsections, several kinds of experiments were briefly summarized. The uni-axial tensile tests along different orientations to the rolling direction were used to identify the planar anisotropy of DP780 sheet. The uni-axial tension with loading–unloading cycles was employed to obtain the degradation of Young's modulus with plastic strain. The cyclic simple shear test, which is a common used technique to calibrate the Bauschinger behavior, was also performed for the purpose of comparison. For the proposed alternative approach, the relevant experiments were described in the other subsections.

3.1. Uni-axial tensile test

Uni-axial tensile tests were carried out on dog-bone samples, each sample with nominal 63.0 mm gauge length, 20.0 mm width, and 1.30 mm initial thickness. Monotonous tensile tests were carried out at 0°, 45°, and 90° to the rolling direction (RD). The deformation gradient **F** in the central zone of the uni-axial tensile specimen is given by

Table 1
Chemical composition *wt*% of DP780 dual phase steel.

	C	Si	Mn	P	Cr	Cu	Mo
DP780	0.073	0.067	2.10	0.0084	0.23	0.0061	0.18

$$\mathbf{F} = F_{xx}e_x \otimes e_x + F_{yy}e_y \otimes e_y + F_{zz}e_z \otimes e_z \tag{7}$$

where e_x denotes the tensile, e_y the transverse and e_z the normal directions, respectively. The test is controlled by the evolution of F_{xx} with time. The engineering strain components ϵ_{xx} and ϵ_{yy}, which are defined as $\epsilon_{xx} = F_{xx} - 1$ and $\epsilon_{yy} = F_{yy} - 1$, are directly measured by digital image correlation system (Tang et al., 2010). A cross-head speed of 3.6 mm/min is imposed which results in an approximate engineering strain rate $\dot{\epsilon}_{xx} = 0.001\ s^{-1}$.

3.2. Uni-axial tension with unloading

In the present work, the Bauschinger behavior will be determined from the springback profile, i.e. the final shape of metallic sheet after being released from the die. As already mentioned, the Young's modulus has a significant influence on the sheet springback (Morestin and Boivin, 1996; Yoshida and Uemori, 2002; Zang et al., 2007). Therefore it is necessary to consider accurately the change of Young's modulus with plastic strain in order to minimize the error resulted from the discrepancy of elastic behavior in numerical simulation.

The uni-axial loading–unloading-reloading tensile test was conducted to quantitatively calibrate the relationship between plastic strain and Young's modulus. The condition for the loading–unloading-reloading tensile test was same as that of monotonic uni-axial tension except the additional unloading–reloading cycles. Preliminary tensile tests were carried out to check the level of uniform elongation. Then the levels of pre-strains were chosen as 1.0%, 1.5%, 2.0%, 3.0%, 4.0%, 5.0%, 6.0%, 7.0%, 8.0%, 9.0%. The method that the same specimen with many unloading-loading cycles was used to avoid the impact of variation of material properties (Sun and Wagoner, 2011). For each unloading–reloading cycle, the continuous unloading was interrupted by the zero stress. The initial Young's modulus is linearly fitted from the true stress vs. strain curve before yielding. The unloading modulus is defined as the slope of a straight line fitting the unloading start point and the end point (σ=0) of the unloading true stress vs. strain curve.

3.3. Cyclic simple shear

The cyclic simple shear test is usually employed to calibrate the Bauschinger behavior of metallic sheet (Bouvier et al., 2006; Thuillier and Manach, 2009). The simple shear device, which was used here, has been described in the author's previous work (Zang et al., 2013b).

The kinematics of the simple shear test can be described by

$$\mathbf{F} = \mathbf{I} + F_{xy}e_x \otimes e_y \tag{8}$$

where $\mathbf{I}$ is the second order identity tensor, e_x is parallel to the shear direction and e_y perpendicular to e_x in the sheet plane. In this work, a specimen with a rectangular gauge area of length b = 25 mm and width h of 5 mm was used. Here the shear direction is along the length direction of this rectangular gauge area. The velocity gradient tensor L for a simple shear deformation, which is defined by $\dot{F} \cdot F^{-1}$, can be written as

$$L = \dot{F}_{xy}e_x \otimes e_y \tag{9}$$

To perform a simple shear deformation with constant velocity gradient tensor, $\dot{F}_{xy}$ must be imposed to a constant value. A cross-head speed of 3.0 mm/min leads to $\dot{F}_{xy}$ of 0.01/s.

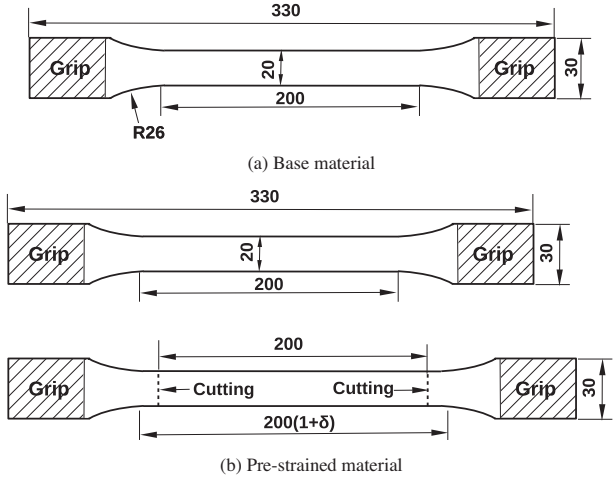

(a) Base material

(b) Pre-strained material

Fig. 3. Dimensions of three-point bending specimen (unit:mm), where δ is the prescribed engineering strain.

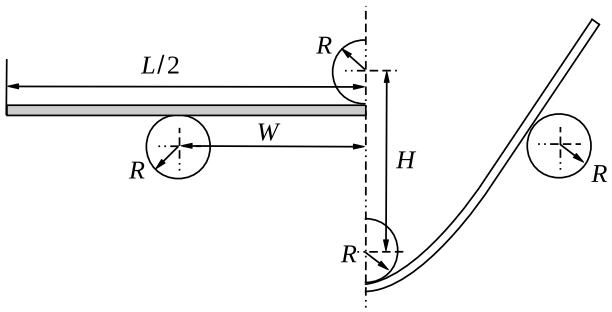

(a) A schematic view of tools and dimensions.

(b) A picture of three-point bending test.

Fig. 4. Three-point bending test.

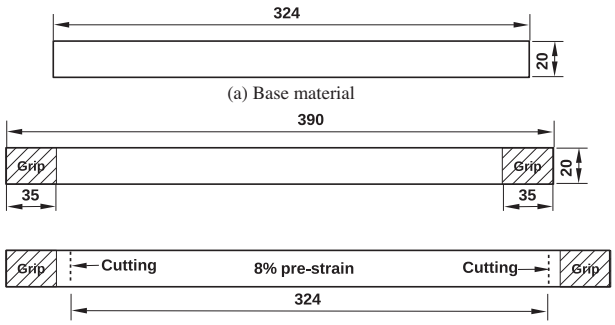

(a) Base material

(b) Pre-strained material

Fig. 5. Dimensions of U-draw/bending specimen (unit:mm).

The shear stress τ_{xy} is given by $\tau_{xy} = Load/bt$, where *Load* is the actual force, and b and t are, respectively, the length and thickness of the specimen. In this work, the cyclic simple shear tests are composed of a loading up to the approximate values of 0.10, 0.19, and 0.25 for the variable F_{xy}, and then followed by a load in the opposite direction until the failure at the shoulder of specimen.

3.4. Three-point bending with pre-strained sheet

A three-point bending test was conducted to obtain the influence of pre-strained tension of metallic sheet on bending springback. The test consists of four procedures as follow. (i) A dog-bone shape specimen (see Fig. 3(a)) with the gauge length of 200 mm was first deformed to a prescribed engineering pre-strain δ, and then unloaded to the zero stress. Similarly as the uni-axial tensile test, the digital image correlation system was used to capture the strain field in the center zone of the specimen. The engineering strain rate is same as that of uni-axial tensile test too. (ii) After that, a rectangular sheet was cut from the pre-strained specimen (see Fig. 3(b)), which is symmetrical to the planar center axis along the width of the dog-bone shape specimen. (iii) Then, the cut rectangular sheet was bended with a standard three-point bending device installed on the material test system. The dimensions of the three-point bending test are illustrated in Fig. 4(a), where the radius R is

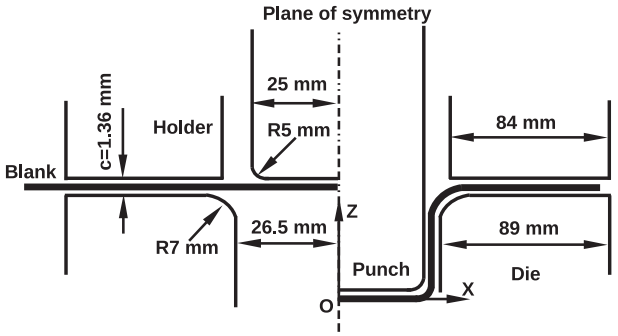

(a) A schematic view of tools and dimensions.

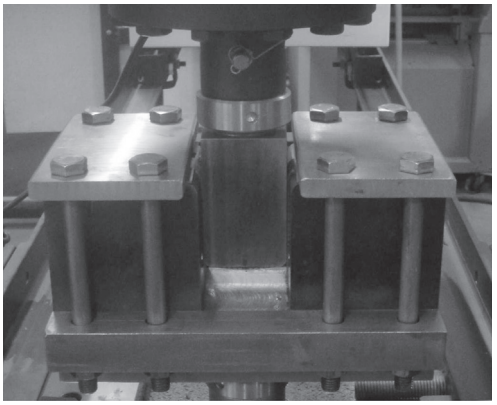

(b) A picture of U-draw/bending test.

Fig. 6. U-draw/bending test.

10 mm, the span W is 40 mm. For the present study, the length of specimen L is 200 mm. As for the maximum stroke H, it is varied to obtain the different bending amounts. A picture of three-point bending test is presented in Fig. 4(b). (iv) Finally, punch was removed after the bending, the final springback profile was obtained.

As already mentioned, the main aim of three-point bending test is to determine the Bauschinger behavior of metallic sheet from bending springback profile. Therefore the three-point bending tests with different pre-strains and maximum strokes are required in the parameters calibration. In this work, three pre-strain amounts and three maximum strokes are designed. The engineering pre-strains are approximate to 4%, 8% and 12%, respectively. Regarding the maximum strokes H, we choose 15 mm, 25 mm and 35 mm in view of dimensions of the present three-point bending test. Consequently, there are nine bending springback profiles in the experimental database of parameters identification.

Furthermore, the three-point bending test is also used to validate the performance of hardening parameters obtained from the new approach. Two engineering pre-strains are designed, i.e. 2% and 9%. A maximum stroke of 30 mm is chosen for each pre-strain. In order to evaluate the directional difference, the three-point bending tests are performed at $0^\circ, 45^\circ$ and 90° to the rolling direction for each pre-strain.

3.5. U-draw/bending test

In U-draw/bending test, the material at sidewall mainly experiences bending, unloading, reverse bending, and unloading, it thus is very suitable to evaluate the hardening model in modeling of mechanical behavior under strain path reversal. This is the reason why the U-draw/bending springback problem has been presented twice in Numisheet benchmark (Nielsen and Brnnberg, 1993; Chung et al., 2011b). In order to validate the hardening model determined from the new approach, as-received and 8% pre-strained specimens were prepared for the DP780 steel sheet. For the base material, 324 mm by 20 mm rectangular shaped specimens were prepared as shown in Fig. 5(a). For the pre-strained material 390 mm by 20 mm, specimens were first deformed in tension with approximate 8% engineering strain schematically represented at the specimen center as measured with an extensometer in Fig. 5(b).

The U-draw/bending test, in Fig. 6, was modified from the version of Numisheet2011 Benchmark 4 (Chung et al., 2011b). The main difference is the way of treating blank holder. The blank holder force is replaced by the blank holder gap which is defined as the fixed clearance between the blank holder and the die surface. Its benefit lies in that we can avoid to measure the blank holder force in the U-draw/bending test. For the present work, two hardened plates with the thickness of 1.36 mm

were placed between the blank holder and die surface for each side, and then four screws are tightly clamped to keep the clearance fixed. Since the blank holder gap is a slight larger than the thickness of DP780 steel sheet, the friction between the blank holder and sheet is almost missed. The friction mainly results from the contact between die round and blank. A lubricant oil was applied to the surface of die round. As for the Coulomb friction coefficient, it will be approximately estimated by comparing the simulated and experimental punch loads. The punch stroke was 72 mm. After the U-draw/bending test, the springback profile was measured. In order to evaluate the directional difference, the specimens at $0^\circ, 45^\circ$ and 90° to the rolling direction were respectively used for each case.

4. Parameter identification

The parameter identification scheme is discussed in this section. For the ANK model, the yield stress $\sigma_\circ$ can be directly determined from the uni-axial tensile test. Although only parameters C_1, γ_1 and C_2 are related to the Bauschinger behavior, it is worth noting that the monotonic hardening behavior is also influenced by the parameter C_2, as depicted in Eq. (6). It means that when the parameter C_2 is adjusted in parameters identification, the monotonic hardening behavior will be changed as well. To keep the monotonic hardening behavior fitted well, the flow stress curve of uni-axial tension along the rolling direction was also added into the experimental database of parameters identification. Therefore the hardening parameters $Q,\ b,\ C_1,\ \gamma_1$ and C_2 are optimized from the measured springback profiles of three-point bending test and the flow stress of uni-axial tension along rolling direction at the same time.

The material parameters identification was performed in an iterative way by minimizing a cost function $\mathscr{L}(A)$. Here the calibration of hardening parameters is carried out with an in-house Matlab toolbox SMAT at Xi'an Jiaotong University. A cost function $\mathscr{L}(A)$ is defined in the least square sense by Eq. (10), and starting from an initial guess of hardening parameters. Then the cost function is minimized.

$$\mathscr{L}(A) = \sum_{n=1}^{N} \mathscr{L}_n(A) = \sum_{\xi} \sum_{\beta} \mathscr{L}_{\xi\beta}^{bending}(A) + \mathscr{L}_{10}^{tension}(A) \tag{10}$$

where n is the number of tests in the database, N is equal to ten for the present parameters identification. Superscript *bending* stands for the springback profile of three-point bending test, *tension* stands for the longitudinal stress in uni-axial tension. ξ and β are respectively assigned to be equal to 1,2 and 3. For the variable ξ, numbers of 1, 2 and 3 correspond to the cases of pre-strains of 4%, 8% and 12%. As for β, numbers of 1, 2 and 3 stand for the conditions of maximum strokes of 15 mm, 25 mm and 35 mm. For each test, the gap between experiment and simulated results is given by

$$\mathscr{L}_n(A) = \frac{1}{M_n} \sum_{i=1}^{M_n} \left(D_n \left| Z(A, t_i) - Z^*(t_i) \right|^2 \right) \tag{11}$$

where M_n is the number of experimental points of the nth test, $Z(A, t_i) - Z^*(t_i)$ is the gap between experimental $Z(A, t_i)$ and simulated result $Z^*(t_i)$ at time t_i, and D_n is a weighting coefficient for the nth test. The experimental database consists of tests with two measured variables, namely stress and coordinate components. A different weighting coefficient is affected for each of these measured variables, the value is chosen according to the uncertainty on the experimental measurement.

For the purpose of comparison, the aforementioned hardening parameters are also identified from the cyclic simple shear test. The following cost function $\mathscr{L}(A)$ is defined

$$\mathscr{L}(A) = \sum_{n=1}^{N} \mathscr{L}_n(A) = \sum_{\xi} \mathscr{L}_n^{tension}(A) + \sum_{\beta} \mathscr{L}_n^{shear}(A) \tag{12}$$

where n is also the number of tests in the database. Superscript *tension* stands for the longitudinal stress in uni-axial tension, *shear* stands for the shear stress in cyclic simple shear. The sum of ξ for tension is performed over all orientations to the rolling direction, β stands for the different pre-strains in cyclic simple shear test.

5. Finite element models

The finite element simulations were carried out with Abaqus version 6.10 (ABAQUS, 2010). All constitutive models used in this work had already been implemented into the Abaqus implicit and explicit codes using the implicit user subroutine UMAT and the explicit user subroutine VUMAT.

For simple shear deformation, its stress state is complicated (Bouvier et al., 2006). It results in that the anisotropy has an influence on the shear stress predicted from the finite element simulation. As already mentioned, the cyclic simple shear tests are also conducted to calibrate the hardening parameters of the ANK model. Therefore it is necessary to describe accurately the anisotropic behavior of metallic sheet. For the purpose of comparison, the non-quadratic anisotropic yield function Yld2000-2d (see Appendix A) was used for all constitutive models in this work due to its good accuracy (Barlat et al., 2003). As for elastic properties, the isotropic elasticity and Poisson's ratio 0.29 were assumed in the numerical simulations.

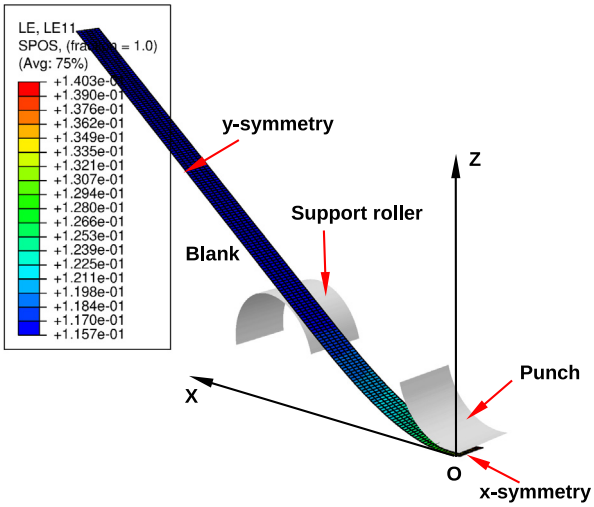

Fig. 7. The deformed configuration in the finite element simulation of the three-point bending test after bending procedure.

5.1. Three-point bending

Five analysis steps are involved in the numerical simulation of the three-point bending test with pre-strained sheet, which are (i) pre-stretching, (ii) unloading, (iii) establishing the contact between the tools and blank, (iv) three-point bending procedure and (v) springback. All these analysis steps were simulated in the implicit code Abaqus/Standard.

To obtain the pre-strained blank, rectangular sheets with a length of 200.0 mm were respectively stretched to the engineering strains of 4%, 8% and 12% in the numerical simulations. It means that the lengths of deformed specimen are 208.0 mm, 216.0 mm or 224.0 mm respectively before unloading. After unloading procedure, the specimen was directly used in the numerical simulation of three-point bending springback problem. Comparing with the length of experimental trimmed specimen (200.0 mm), we believe that there is no impact from the present simplicity because the plastic deformation in three-point bending test mainly occurs at the blank between two supported rollers.

Considering the symmetry of the model and boundary condition, a quarter of the rectangular blank was simulated. The analytical rigid-body element was chosen for the tools. The reduced 4-node shell element (S4R) was employed for the blank. A mesh size of 0.5 mm $\times$ 1.0 mm (length $\times$ width) and 21 Simpson integration points through the thickness were chosen. The Coulomb friction coefficient between tools and the blank was assumed to be 0.1 due to the fact that the two supported rollers cannot rotate in experiment. The deformed configuration in the finite element simulation of the three-point bending test after bending procedure is illustrated in Fig. 7. For the convenience, the predicted springback profile is expressed in the Cartesian coordinate of *OXZ* as defined in Fig. 7.

5.2. U-draw/bending

In the numerical simulation of U-draw/bending test, four analysis steps are involved, which are (i) pre-strain, (ii) unloading, (iii) U-draw/bending procedure and (iv) springback. The first two analysis steps were first simulated in the Abaqus/Standard. Then the deformed state was imported into the Abaqus/Explicit to simulate the forming procedure, and finally the state after forming was again imported into the Abaqus/Standard to simulate the springback.

For the base material, 324 mm by 20 mm rectangular shaped specimen was directly used in numerical simulation of U-draw/bending test. As for the pre-strain case, the specimen with a length of 300 mm was first stretched to the engineering strain of 8%. It indicates that the length of pre-strained specimen is 324 mm before unloading. After unloading procedure, the specimen was then used in the numerical simulation of forming procedure. Taking symmetry into consideration, only a quarter of the whole rectangular blank was simulated. The tools were constructed with analytical rigid body surface. The blank was simulated using reduced 4-node shell element (S4R) and 9 integration points through thickness. The mesh size was chosen as 0.5 mm by 0.5 mm (length by width). Since the fixed large clearance (1.36 mm) between blank holder and die is used, we believe that the influence of friction on predicted springback is not significant comparing with that of constant blank holder force. To approximately estimate the coefficient of Coulomb friction law, the predicted punch load vs. stroke curves from ANK model with different friction coefficients are qualitatively compared with experimental result. Then the estimated friction coefficient was employed in the following springback predictions of U-draw/bending tests.

Table 2
Coefficients of Yld2000-2d anisotropic yield function.

Material	Parameters	Values
DP780	α_1	0.9685
	α_2	0.9909
	α_3	1.0343
	α_4	1.0057
	α_5	1.0284
	α_6	1.0438
	α_7	0.9935
	α_8	0.9821
	m	6.0

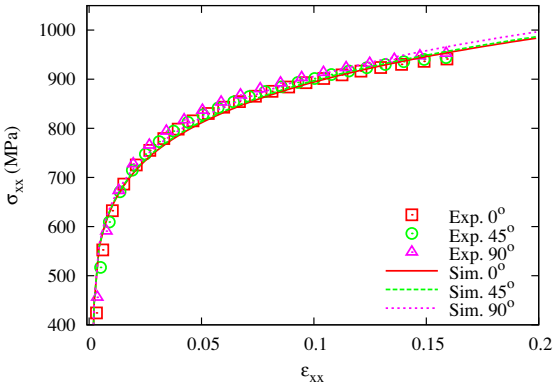

(a) The true stress vs. strain

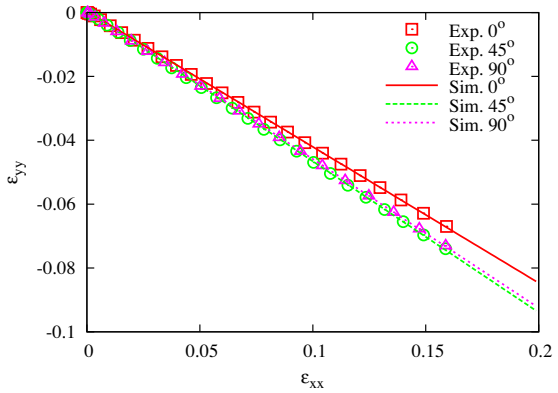

(b) Evolution of transverse strain with longitudinal strain

Fig. 8. The experimental and simulated results in uni-axial tension for DP780 steel sheet, where the constitutive model incorporating Yld2000-2d anisotropic yield function with a Swift-type isotropic hardening law is used to predict the mechanical behavior.

6. Results and discussion

The material parameters of the current constitutive model can be categorized into three aspects, the coefficients of Yld2000-2d anisotropic yield function, the parameters related to the change of unloading modulus and hardening parameters. As already mentioned, the hardening parameters related to the Bauschinger behavior are determined from the spring-back profiles of three-point bending tests in the new approach. For the purpose of comparison, the same hardening parameters are also identified by the simple shear test. Therefore it is better to minimize the errors resulted from the planar anisotropy and the change of unloading modulus.

For the planar anisotropy, it is captured by the Yld2000-2d anisotropic yield function in the present work. The material coefficients of the anisotropic yield function is usually calibrated from the experimental initial yield stresses and r-values in uni-axial tension tests and bi-axial tensile stress and r-value (Barlat et al., 2003). However, as already pointed out, the initial yield stresses determined at a very small plastic strain might not reflect the subsequent anisotropy of the metallic sheet at

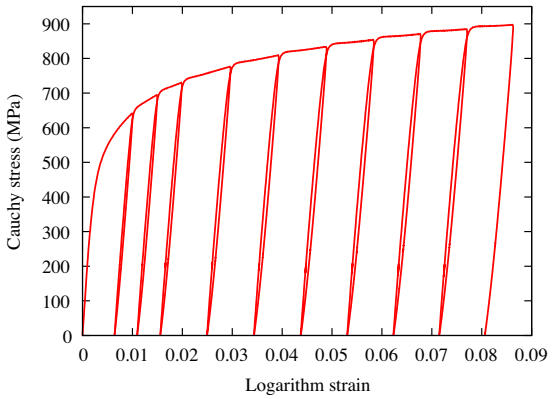

Fig. 9. Results of uni-axial tensile test with loading–unloading cycles.

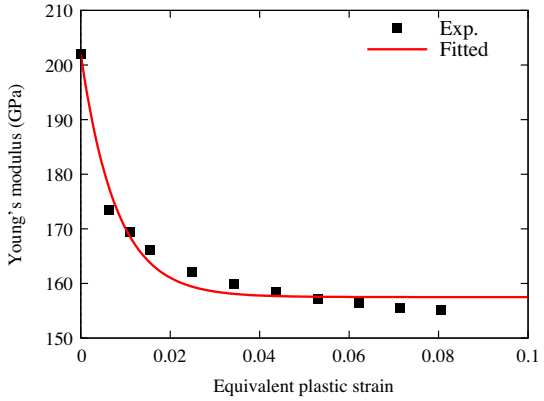

Fig. 10. Unloading modulus vs. equivalent plastic strain in the uni-axial tension state.

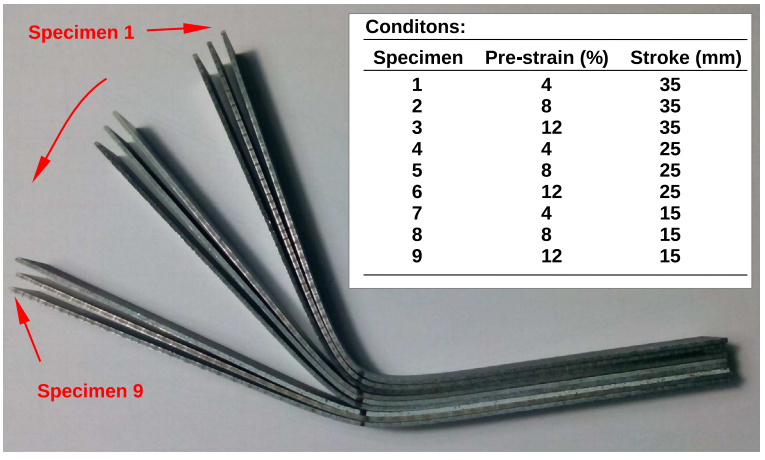

Fig. 11. Samples after the three-point bending at different pre-strains and maximum strokes.

larger strains (Barlat et al., 2005). To compromise the initial and subsequent anisotropy, the coefficients α_i (i = 1–8) of Yld2000-2d anisotropic yield function were optimized from both the stress vs. strain and transverse strain vs. longitudinal strain curves of uni-axial tension at 0°, 45° and 90° to the rolling direction. This identification strategy of material coefficients of Yld2000-2d anisotropic yield function might lose some accuracy on the description of initial anisotropy, but gains more accuracy in the prediction of initial and subsequent anisotropy (Zang et al., 2011b). In addition, because the flow stress and

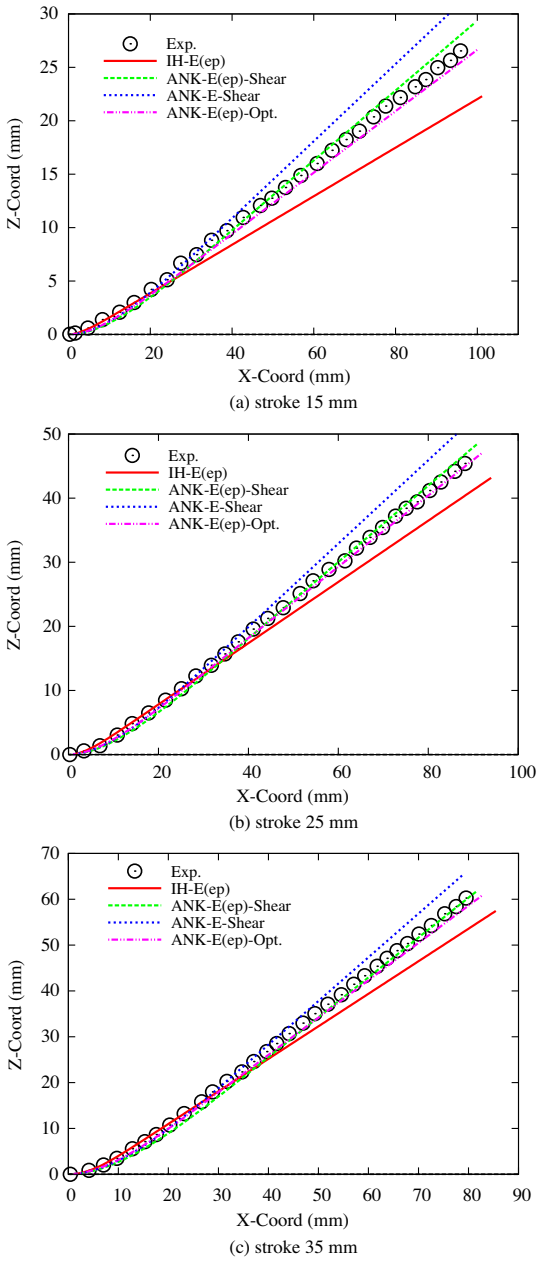

Fig. 12. Experimental and predicted springback profiles of the three-point bending tests for the engineering pre-strain of 4%.

evolution of transverse strain in uni-axial tension are used to optimized the coefficients of Yld2000-2d yield function, an isotropic hardening model is also needed to capture the global hardening behavior. Here we choose a Swift type isotropic hardening equation to describe the flow stress of uni-axial tensile test. The equation is defined as $\bar{\sigma}(\bar{\varepsilon}^p) = K(\varepsilon_0 + \bar{\varepsilon}^p)^n$ with $\varepsilon_0 = (\sigma_0/K)^{1/n}$, where K and n are hardening parameters, σ_0 is the initial yield stress in reference direction. At present, the number of unknown material parameters for the identification is eleven, i.e. eight material coefficients of Yld2000-2d anisotropic yield function and three hardening parameters of Swift isotropic hardening law. However, note that there is a constraint for the material coefficients of Yld2000-2d anisotropic yield function so that the predicted flow stress from constitutive model is equal to that from the Swift-type isotropic hardening equation. For simplicity, the initial yield stress σ_0 is not optimized, but the measured experimental one is used. For the present DP780 steel sheet, the experimental initial yield stress σ_0 is 498.8 MPa. As for the other ten material parameters, the identified material coefficients of Yld2000-2d anisotropic yield function are listed in Table 2, hardening parameters K and n are 1228.8 MPa and 0.135, respectively.

Finally, the experimental and simulated Cauchy stress and transverse strain in uni-axial tension are shown in Fig. 8. It can be seen that the differences of experimental flow stresses for the DP780 steel sheet are not distinct (see Fig. 8(a)). However,

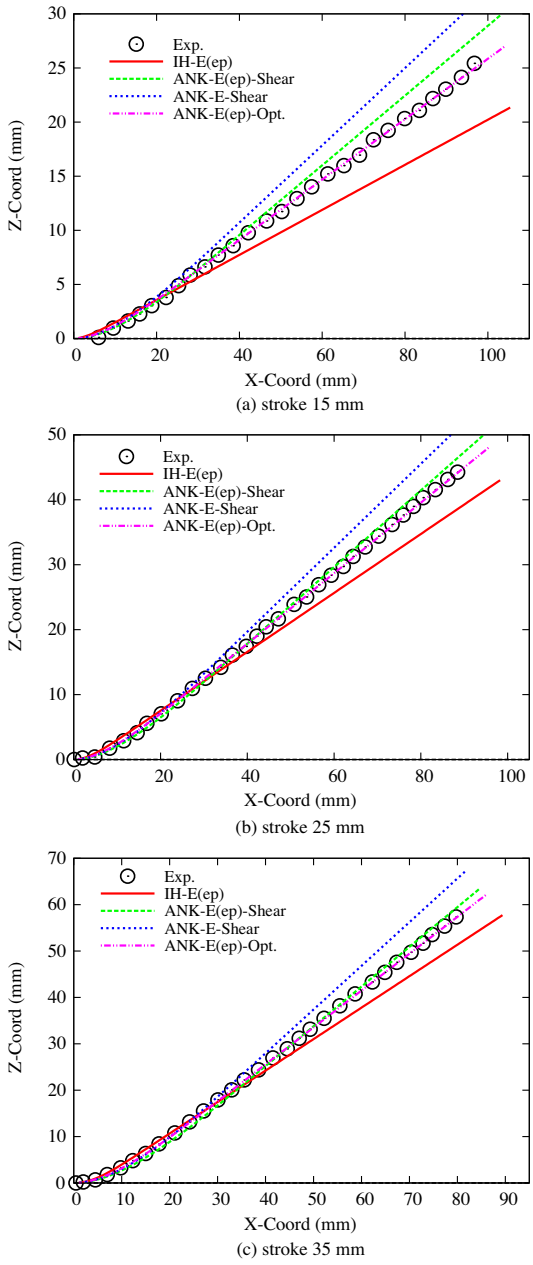

Fig. 13. Experimental and predicted springback profiles of the three-point bending tests for the engineering pre-strain of 8%.

for the experimental plastic anisotropy, the gap is obvious as shown in Fig. 8(b). The simulated Cauchy stresses and transverse strains from Yld2000-2d anisotropic yield function coincide with the experiments well. Thus we can consider the material coefficients of Yld2000-2d anisotropic yield function listed in Table 2 have captured well the planar anisotropy of DP780 steel sheet. In the following parameters identification of hardening model, the material coefficients provided in Table 2 will be used in order to minimize the influence of planar anisotropy.

As for the influence of pre-strain on unloading modulus, the experimental Cauchy stress of uni-axial tension with intermediate unloading cycles is presented in Fig. 9. It can be seen that the unloading and reloading curves in each cycle are non-linear, and their difference is obvious. The experimental investigation indicates that this physical phenomenon of non-linear unloading is not purely elastic or plastic (Sun and Wagoner, 2011). To model the non-linear unloading behavior, a new concept of quasi-plastic-elastic (QPE) strain was introduced within the continuum framework (Sun and Wagoner, 2011). Here, for simplicity, the so-called chord modulus model was adopted to calculate the experimental unloading modulus (Sun and Wagoner, 2011; Kim et al., 2013). To consider the effect of pre-strain on unloading modulus, Yoshida et al. (2002) and Yamaguchi et al. (1998) assumed that unloading modulus can be expressed as a scalar function of the equivalent plastic

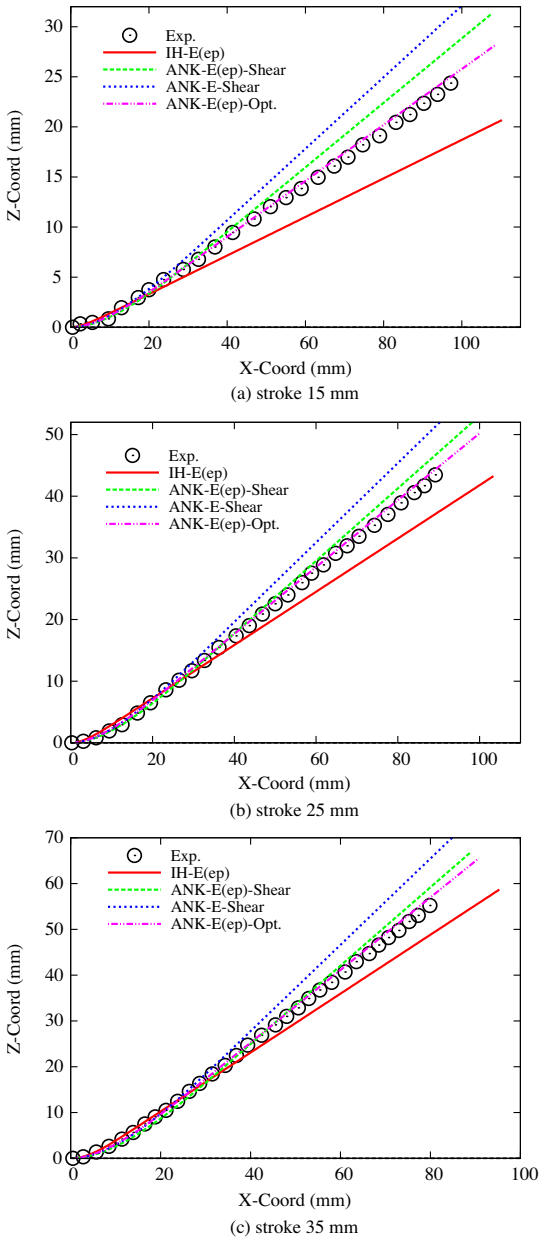

Fig. 14. Experimental and predicted springback profiles of the three-point bending tests for the engineering pre-strain of 12%.

strain. To formulate such a pre-strain dependency of unloading modulus, they proposed a saturated type function of equivalent plastic strain which has been widely used (e.g. Yoshida et al., 2002; Zang et al., 2007; Lee et al., 2012b; Kim et al., 2013). Usually, the unloading modulus is formulated as an exponential equation

$$E = E_0 - (E_0 - E_{sat})[1 - e^{(-\xi \bar{\varepsilon}^p)}] \tag{13}$$

where E_{sat} and ξ are two material parameters, E_{sat} is the saturated elastic modulus, E_0 is the initial Young's modulus. From the uni-axial tensile test, the measured initial Young's modulus of DP780 steel sheet is 202.07 GPa. By fitting the measured unloading modulus with Eq. (13), E_{sat} and ξ can be obtained, which are 157.51 GPa and 126.38, respectively. The measured and fitted unloading modulus vs. equivalent plastic strain is shown in Fig. 10. It can be seen that the unloading modulus rapidly decreases and saturates to E_{sat} as the equivalent plastic strain increases. For the critical equivalent plastic strain, it is very small and around 0.03.

Table 3
Material parameters of the hardening models for DP780 steel sheet.

Parameter	Unit	ANK-E (ep)-Shear	ANK-E (ep)-Opt.
$\sigma_\circ$	MPa	498.8	498.8
C_1	MPa	40433.8	31216.65
γ_1	–	94.7	101.62
C_2	MPa	468.8	521.87
Q	MPa	360.9	354.20
b	–	51.5	49.01

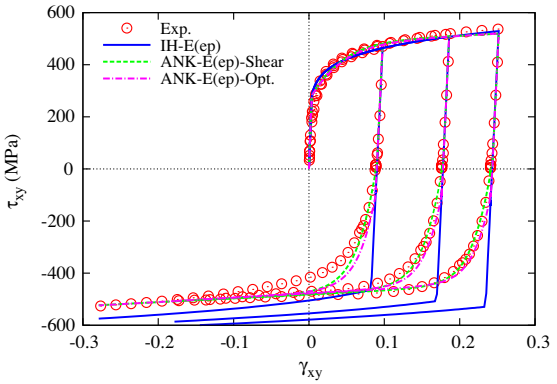

Fig. 15. The experimental and predicted Cauchy stress in simple shear test at different amounts of forward shear along the rolling direction.

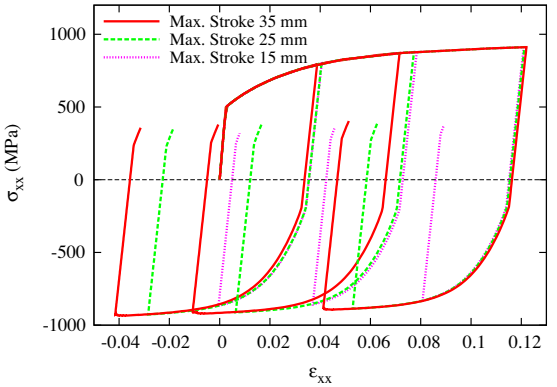

Fig. 16. The predicted Cauchy stress evolution of the blank element at the inner surface of the three-point bending.

As already explained in Section 2, for a pre-strained sheet, its cyclic mechanical behavior has an influence on the bending moment before unloading. Since the springback is uniquely determined by bending moment, it can be inferred that the pre-strain has an effect on the final springback profile of three-point bending test too. The samples after the three-point bending tests with different pre-strains and maximum strokes are shown in Fig. 11. Here it is worth noting that the pre-strains are approximate due to the fact that the digital image correlation system was not real-time to calculate the strain field. The exact pre-strains are applied in the numerical simulations of the uni-axial tension. It can be seen from Fig. 11 that the springback is more serious with the increasing of pre-strains among all cases of maximum strokes. This can be explained as that the effect of pre-strain actually changes the material property by hardening (Hemmerich et al., 2011). The pre-strained sheet has higher strength, which results in the larger springback.

Figs. 12–14 are the experimental and predicted springback profiles of the three-point bending tests at different pre-strains. Here the notation *IH-E*(*ep*) stands for the springback profile simulated by an isotropic hardening model incorporating with the change of Young's modulus with plastic strain. For *ANK-E-Shear* and *ANK-E*(*ep*)*-Shear*, they represent the simulated results from the ANK model without/with the variations of Young's modulus, where *Shear* means that the hardening parameters are calibrated from the cyclic simple shear test. As for *ANK-E*(*ep*)*-Opt.*, it stands for the simulated springback from the ANK model and varied Young's modulus, where *Opt.* means that the hardening parameters of the ANK model are optimized

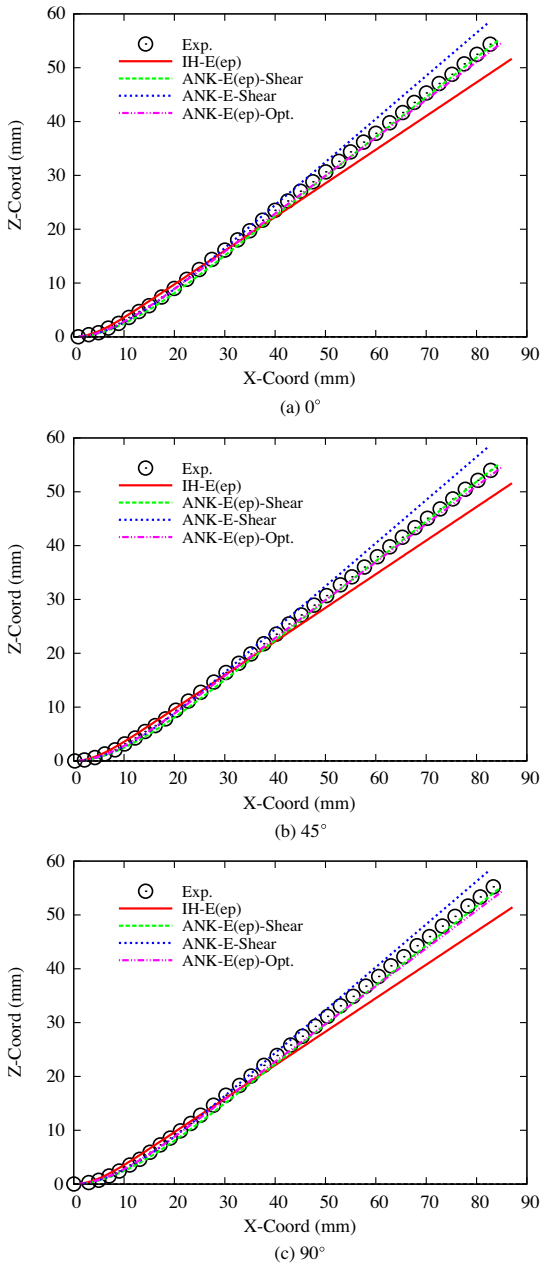

Fig. 17. Experimental and predicted springback profiles of the three-point bending tests (stroke 30 mm) for the engineering pre-strain of 2%.

from the three-point bending springback profiles. It can be seen that the isotropic hardening model incorporating with the change of Young's modulus over-estimates the springback as expected. While the constitutive model of *ANK-E-Shear* under-estimates the springback profile of three-point bending test. This is because the ANK model predicts a lower springback comparing with that of pure isotropic hardening model. Meanwhile, the constant Young's modulus makes the simulated springback lower than that of varied Young's modulus as well. Such a relative relationship has been discussed in author's previous work (Zang et al., 2013a) when the unloading modulus is introduced in sheet springback prediction. The predicted springback profile from the model of *ANK-E(ep)-Shear* has a good agreement with the experimental result. In particular, the simulated springback profiles from the ANK model incorporating with the changed Young's modulus, where hardening parameters are optimized from the new approach, coincide with the experimental profiles very well. It indicates that the cost function defined in Eq. (10) has been minimized. Even though the isotropic elasticity was assumed in the parameters identification, the directional Young's modulus is suggested to be measured when the three-point bending

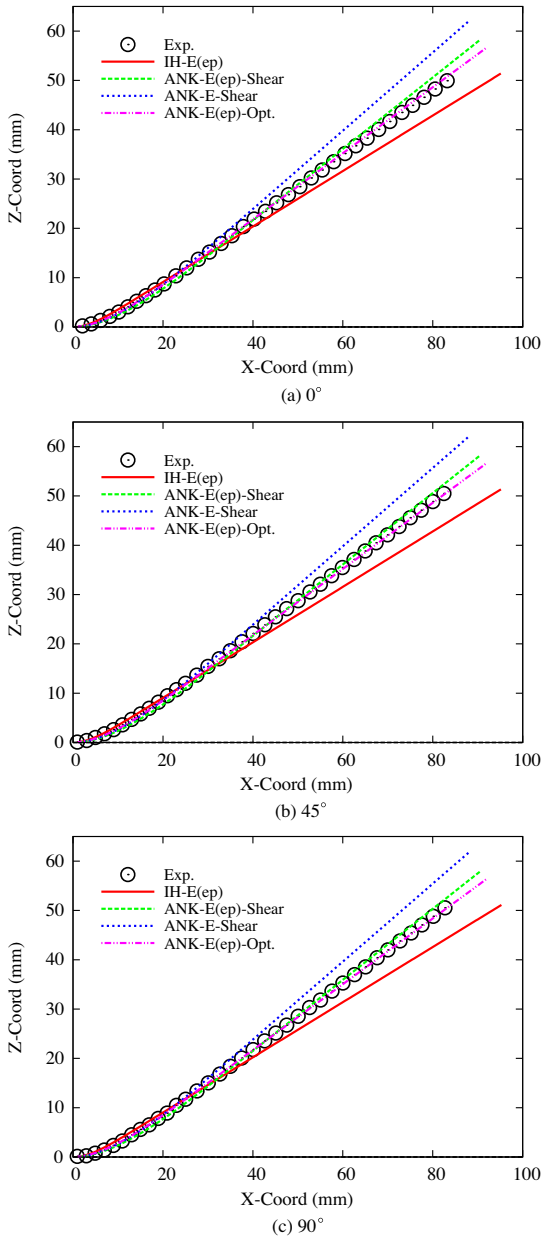

Fig. 18. Experimental and predicted springback profiles of the three-point bending tests (stroke 30 mm) for the engineering pre-strain of 9%.

tests are performed for the specimens in different directions. This is because the elastic deformation is dominant in three-point bending as discussed in the work of Chung et al. (2011a).

Using the hardening parameters calibrated from the cyclic simple shear test and the new approach, as listed in Table 3, the experimental and predicted shear stresses τ_{xy} in simple shear deformation along the rolling direction are compared in Fig. 15. It can be seen that the pure isotropic hardening model *IH-E*(*ep*) predicts a large shear stress under reverse loading as usual. The shear stress τ_{xy} simulated by the hardening parameters, which are optimized from the new approach, is almost same as that of cyclic simple shear test. However, the shear stress at the early re-yielding stage predicted from the new approach is slight larger than that of cyclic simple shear test. This is because the magnitude of reverse deformation is small at the early re-yielding stage. In the three-point bending test for a pre-strained sheet, the material, which experiences such a slight deformation, is usually near the neutral layer. Thus it has a slight contribution to the bending moment.

To check the magnitude of compressive deformation $\varepsilon_{bending}$ as depicted in Fig. 2(b), the predicted Cauchy stress σ_{xx} of the blank element at the inner surface of the three-point bending is shown in Fig. 16. For different maximum strokes, the magnitudes of compressive strains are obviously different. The compressive strain corresponding to the maximum stroke of

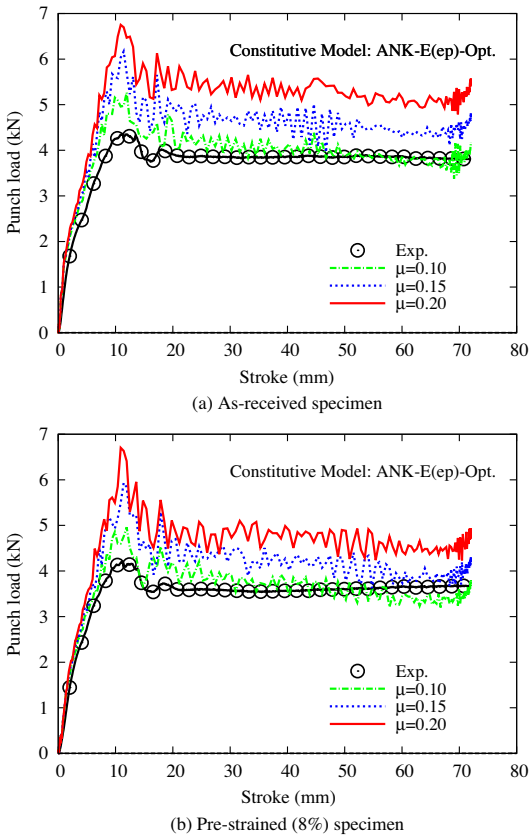

Fig. 19. Influence of friction coefficient on load vs. stroke curves of the U-draw/bending test.

35 mm is approximate to 0.07. It can be inferred that the compressive strain can be increased with the smaller punch radius, larger maximum stroke or smaller span between two supported rollers. By choosing different pre-strains $\varepsilon_{prestrain}$ and compressive strains in bending $\varepsilon_{bending}$ (see Fig. 2(b)), the cyclic mechanical behavior with wide ranges of compressive strain will be involved in the experimental springback profiles. Then the hardening parameters related to the Bauschinger behavior can be simply determined from these springback profiles by using an inverse method.

To validate the performance of hardening parameters determined from the new approach, the three-point bending and U-draw/bending tests were also conducted. Figs. 17 and 18 are the experimental and predicted springback profiles of the three-point bending tests with the pre-strains 2% and 9%. It can be seen that the ANK model with changed Young's modulus results in good predictions for both cases no matter which method we use to determine the Bauschinger effect. However, the discrepancy of simulated springback from *ANK-E(ep)-Shear* and *ANK-E(ep)-Opt.* models for the pre-strain of 9% is larger than those of 2% pre-strain. For the present ANK model, the hardening behavior under uni-axial loading only relates to the parameters C_2, Q and b (Zang et al., 2011a, 2013a). Table 3 shows that the differences of these hardening parameters are not obvious. Since the hardening behavior of the material with a small reversal pre-strain is more like that of monotonic loading, the springback predicted from the aforementioned two models should be close too. As for the pre-strain of 9%, Fig. 18 indicates that the hardening parameters obtained from the new approach can give better springback predictions comparing with those of simple shear test.

For the U-draw/bending test, the experimental and simulated punch load vs. stroke curves are compared in order to approximately estimate the friction coefficient as shown in Fig. 19. It can be seen that the simulated load vs. stroke curves with the coefficient 0.1 fit the experimental results well. As already mentioned, the friction might have a slight influence on springback prediction in the case of large blank holder gap. Therefore the Coulomb friction law was assumed with the coefficient 0.1 between the blank and tools in the following numerical simulations of U-draw/bending tests. Fig. 20 is the experimental and simulated springback profiles of the U-draw/bending tests at 0°, 45° and 90° to the rolling direction. It can be seen that the discrepancy of simulated springback at punch round from *IH-E(ep)* model and all ANK models is small for the as-received specimen, while the gaps are comparatively large for the pre-strained specimen. The inner material near the punch round in the U-draw/bending test mainly experiences compressive deformation along the tangential direction. For the pre-strained specimen, the whole deformation history of the material is thus tension and subsequent compression. As already explained in Section 2, the springback of a uni-axially tensioned strip is strongly influenced by the Bauschinger

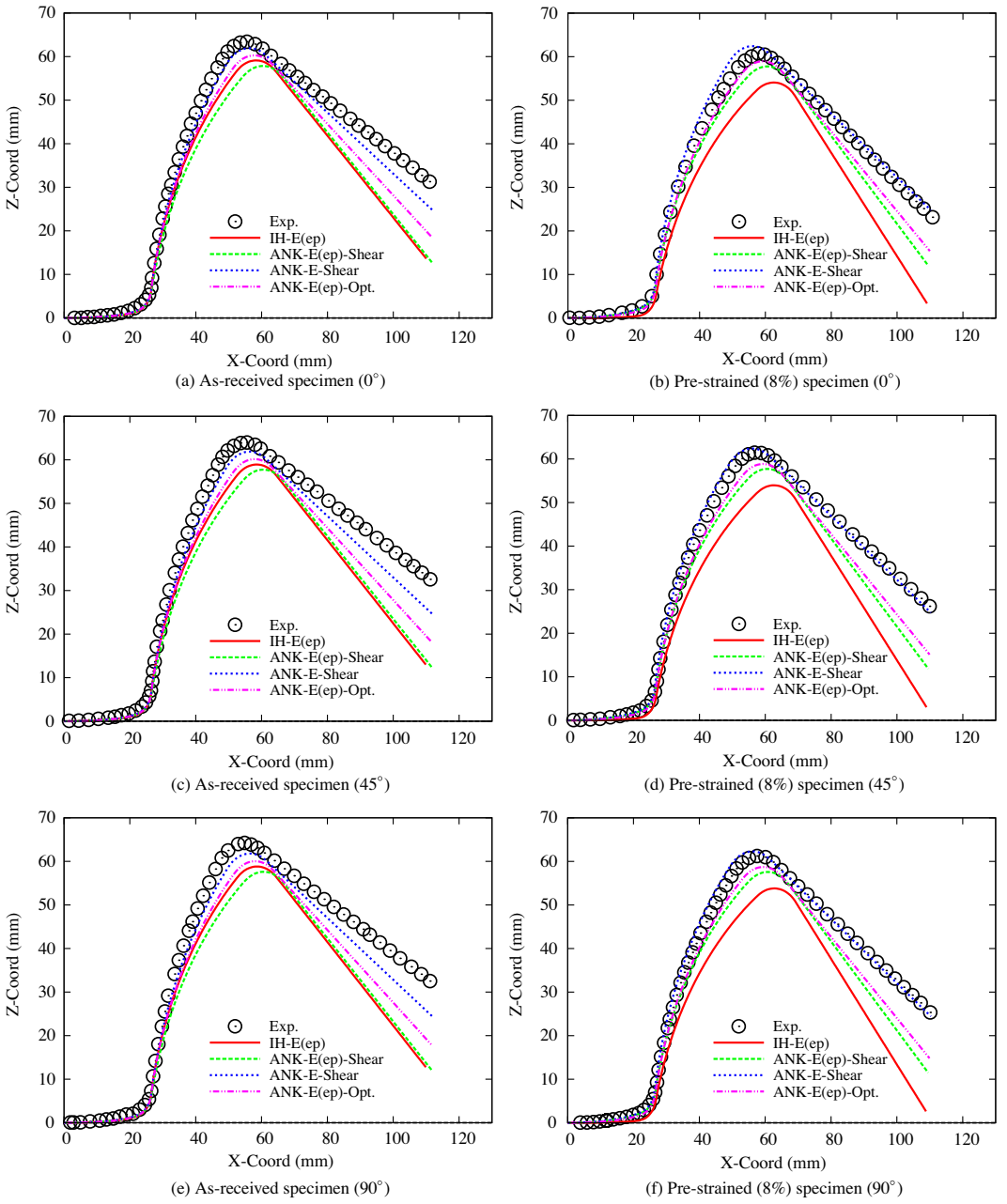

Fig. 20. Experimental and predicted springback profiles of the U-draw/bending tests.

behavior of the material. The aforementioned discrepancy confirms the validity of the proposed approach since the isotropic hardening model cannot reproduce the Bauschinger behavior.

Furthermore, even though the springback profiles predicted by *ANK-E(ep)-Opt.* model are more close to the experimental results comparing with those of *ANK-E(ep)-Shear* model, it is worth noting that both *ANK-E(ep)-Shear* and *ANK-E(ep)-Opt.* models overestimate the springback. We think the adopting chord modulus might be one possible reason for such a significant discrepancy. The work by Sun and Wagoner (2011) showed clearly that adopting a chord modulus is not sufficient in springback cases when the unloading ends up at a range of stresses. This is because the effective unloading modulus for each material point is then different, not based on pre-strain only, but on final stress. To clarify it, the effective unloading modulus is schematically illustrated by taking uni-axial tension as an example as shown in Fig. 21. If the final stress after unloading is not equal to zero, it can be seen that the effective unloading modulus should be larger than that of zero final stress. Considering the level of final stress in U-draw/bending test, the change of Young's modulus with plastic strain was re-calculated from the Fig. 9 based on the final stress of κ=0.25. Then improved springback predictions were obtained as shown in

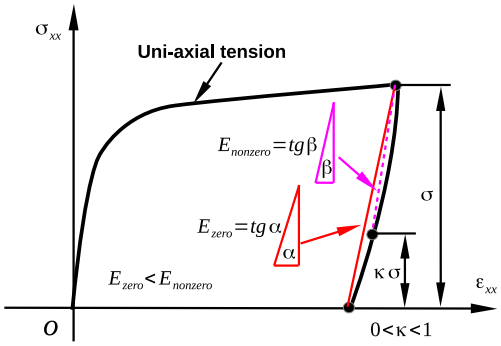

Fig. 21. A schematic illustration on the chord modulus fitted from different unloading stress–strain curves in uni-axial loading.

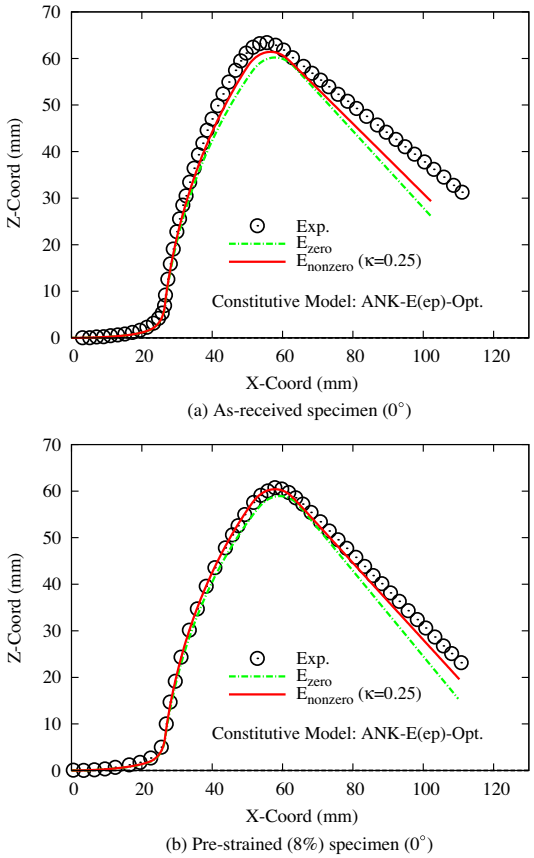

Fig. 22. Experimental and predicted springback profiles of the U-draw/bending tests with the re-calculated Young's modulus.

Fig. 22. It is worth noting that the effective unloading modulus for each material point is different in the U-draw/bending test. In this sense, the springback predicted with this recalculated Young's modulus is not rigorous. But it could provide a reasonable explanation on the reason of this discrepancy. It can be inferred that the prediction of springback will be more accurate if the non-linear unloading behavior is accounted for. Furthermore, even though some recent advanced constitutive models incorporating with non-linear unloading behavior have resulted in good predictions for most materials (Sun and Wagoner, 2011; Lee et al., 2013), we can find that there is still a slight discrepancy in some cases for advanced high strength steels (Lee et al., 2013). It indicates that many aspects of constitutive model should be considered in modeling of sheet springback, for instances measurement and modeling of hardening behavior, non-linear unloading, initial and subsequent anisotropy. Considering the main purpose of present work, the new approach is simple and promising for the measurement of the Bauschinger behavior when the constitutive framework has been established well.

7. Conclusion and future works

This paper presents an alternative approach to determine the Bauschinger behavior from three-point bending springback with pre-strained sheets. For a pre-strained sheet, the further bending makes the inner material experienced tension and compression. Therefore the cyclic mechanical behavior of metallic sheet has an influence on the bending moment and final springback. Utilizing this feature, the material parameters corresponding to the aforementioned hardening behavior can be inversely calibrated from the final springback profiles of the three-point bending tests with different pre-strained sheets. For the new approach, in particular, the change of Young's modulus should be captured accurately due to the fact that springback is also significantly influenced by elastic properties. Taking the DP780 steel sheet as an example, its hardening parameters of the ANK model were calibrated respectively from the cyclic simple shear test and the new approach. Moreover the U-draw/bending test was employed to validate the performance of determined hardening parameters. The results have confirmed the validity of the suggested new approach. With the increasing applications of advanced high strength steels, the new approach provides a simple and promising way to obtain the Bauschinger behavior since the springback is distinct for the advanced high strength steels.

Regarding the new approach, it is worth noting that the constitutive framework should be already well-established for the used material. This is because the new approach is very similar to the bending-reverse bending method to calibrate the Bauschinger behavior. For such bending-type tests, we cannot directly measure the cyclic mechanical behavior under uni-axial loading, whereas the bending moment is essentially used in parameters identification. As already known, the bending moment is integrated from the stress distribution through thickness direction of the metallic sheet. This leads to the possibility that same bending moment might relate to different stress distributions. To minimize the possibility, two aspects need to be considered at least. Firstly, the cyclic mechanical behavior of the used material has been recognized well, and the selected constitutive model can capture the aforementioned behavior accurately as already mentioned. Secondly, the experimental data at different ranges of bending strain should be included in parameters identification. In future work, the cylindrical bending, three-point bending and V-bending tests might be respectively adopted to achieve the maximum bending strains at small, moderate and large scales. Moreover, a systematic investigation is also required to understand if the new approach can give a unique constitutive model within certain range of strains.

Furthermore, the addition of non-linear unloading behavior provides a new dimension of the constitutive model in present parameters identification, among which many choices may be able to reproduce the experimental bending results with or without pre-strain. The adopted chord modulus is not sufficient in complicated springback problems when the unloading ends up at a range of stresses as already pointed by Sun and Wagoner (2011). There is no doubt that the better way is to describe the non-linear unloading behavior accurately by using advanced constitutive models, for instance the QPE model (Sun and Wagoner, 2011; Lee et al., 2013). Although the springback profiles are employed to calibrate the Bauschinger behavior in the present work, we want to point out that the punch load of three-point bending test could be adopted in parameters identification instead of springback profile.

Acknowledgments

Shun-lai Zang would like acknowledge financial support by the General Motors China Science Lab (CSL-040), the National Natural Science Foundation of China (No. 11002105) and the Opening Project of Key Laboratory of Testing Technology for Manufacturing Process (Southwest University of Science and Technology), Ministry of Education (No. 10ZXZK03). Professor Jin Liang of Xi'an Jiaotong University kindly provided the digital image correlation system XJTUDIC™. Jun-hua Liu of Xi'an Jiaotong University is also thanked for her assistance during the experiments. Myoung-Gyu Lee appreciates the supports from ISTK for the project on "pulsed electrical assisted forming technology" and ERC program funded by the Korea government (MSIP) (No. 2012R1A5A1048294).

Appendix A. Anisotropic yield function Yld2000-2d

The non-quadratic anisotropic yield function Yld2000-2d is a linear transformation of two convex functions ϕ' and ϕ'' (Barlat et al., 2003). It is defined by an equivalent stress $\bar{\sigma}$:

$$\phi(s) = \bar{\sigma} = \left[\frac{1}{2}(\phi' + \phi'')\right]^{\frac{1}{m}} \tag{A-1}$$

where

$$\phi' = |S'_1 - S'_2|^m; \quad \phi'' = |2S''_2 + S''_1|^m + |2S''_1 + S''_2|^m \tag{A-2}$$

with $m = 6$ and $m = 8$ for BCC and FCC materials, respectively. $S'_{1,2}$ and $S''_{1,2}$ are the principal values of the linear transformations on the stress deviator tensors $\tilde{s}'$ and $\tilde{s}''$. The principal values $S_{1,2}$ of the transformed stress deviator tensor $\tilde{s}$ are respectively defined as

$$S_1 = \frac{1}{2}\left(\tilde{s}_{11} + \tilde{s}_{22} + \sqrt{(\tilde{s}_{11} - \tilde{s}_{22})^2 + 4\tilde{s}_{12}^2}\right) \tag{A-3a}$$

$$S_2 = \frac{1}{2}\left(\tilde{s}_{11} + \tilde{s}_{22} - \sqrt{(\tilde{s}_{11} - \tilde{s}_{22})^2 + 4\tilde{s}_{12}^2}\right) \tag{A-3b}$$

The transformed stress deviator tensors $\tilde{s}'$ and $\tilde{s}''$ are calculated from

$$\tilde{s}' = \boldsymbol{L}' \cdot \boldsymbol{\sigma}; \quad \tilde{\boldsymbol{s}}'' = \boldsymbol{L}'' \cdot \boldsymbol{\sigma} \tag{A-4}$$

Here the tensors $\boldsymbol{L}'$ and $\boldsymbol{L}''$ representing linear transformation of the stress tensor are

$$\begin{bmatrix} L'_{11} \\ L'_{12} \\ L'_{21} \\ L'_{22} \\ L'_{66} \end{bmatrix} = \begin{bmatrix} 2/3 & 0 & 0 \\ -1/3 & 0 & 0 \\ 0 & -1/3 & 0 \\ 0 & 2/3 & 0 \\ 0 & 0 & 1 \end{bmatrix} \begin{bmatrix} \alpha_1 \\ \alpha_2 \\ \alpha_7 \end{bmatrix} \tag{A-5a}$$

$$\begin{bmatrix} L''_{11} \\ L''_{12} \\ L''_{21} \\ L''_{22} \\ L''_{66} \end{bmatrix} = \frac{1}{9}\begin{bmatrix} -2 & 2 & 8 & -2 & 0 \\ 1 & -4 & -4 & 4 & 0 \\ 4 & -4 & -4 & 1 & 0 \\ -2 & 8 & 2 & -2 & 0 \\ 0 & 0 & 0 & 0 & 9 \end{bmatrix} \begin{bmatrix} \alpha_3 \\ \alpha_4 \\ \alpha_5 \\ \alpha_6 \\ \alpha_8 \end{bmatrix} \tag{A-5b}$$

where all the independent coefficients α_k (for k:1–8) are material parameters to describe the anisotropy.

References

ABAQUS, 2010. User's manual (version 6.10). Hibbit, Karlsson & Sorensen Inc., USA.

Andar, M.O., Kuwabara, T., Steglich, D., 2012. Material modeling of AZ31 mg sheet considering variation of r-values and asymmetry of the yield locus. Mater. Sci. Eng.: A 549, 82–92.

Barlat, F., Brem, J., Yoon, J., Chung, K., Dick, R., Lege, D., Pourboghrat, F., Choi, S.H., Chu, E., 2003. Plane stress yield function for aluminum alloy sheets part 1: theory. Int. J. Plast. 19, 1297–1319.

Barlat, F., Aretz, H., Yoon, J., Karabin, M., Brem, J., Dick, R., 2005. Linear transfomation-based anisotropic yield functions. Int. J. Plast. 21, 1009–1039.

Boger, R., Wagoner, R., Barlat, F., Lee, M., Chung, K., 2005. Continuous, large strain, tension/compression testing of sheet material. Int. J. Plast. 21, 2319–2343.

Bouvier, S., Haddadi, H., Leve, P., Teodosiu, C., 2006. Simple shear tests: experimental techniques and characterization of the plastic anisotropy of rolled sheets at large strains. J. Mater. Process. Technol. 172, 96–103.

Cao, J., Lee, W., Cheng, H.S., Seniw, M., Wang, H.P., Chung, K., 2009. Experimental and numerical investigation of combined isotropic-kinematic hardening behavior of sheet metals. Int. J. Plast. 25, 942–972.

Carbonnire, J., Thuillier, S., Sabourin, F., Brunet, M., Manach, P., 2009. Comparison of the work hardening of metallic sheets in bending unbending and simple shear. Int. J. Mech. Sci. 51, 122–130.

Chaboche, J.L., 1986. Time-independent constitutive theories for cyclic plasticity. Int. J. Plast. 2, 149–188.

Chaboche, J., 2008. A review of some plasticity and viscoplasticity constitutive theories. Int. J. Plast. 24, 1642–1693.

Chun, B., Jinn, J., Lee, J., 2002. Modeling the bauschinger effect for sheet metals, part i: theory. Int. J. Plast. 18, 571–595.

Chung, K., Park, T., 2013. Consistency condition of isotropic kinematic hardening of anisotropic yield functions with full isotropic hardening under monotonously proportional loading. Int. J. Plast. 45, 61–84.

Chung, K., Lee, M.G., Kim, D., Kim, C., Wenner, M.L., Barlat, F., 2005. Spring-back evaluation of automotive sheets based on isotropic-kinematic hardening laws and non-quadratic anisotropic yield functions: part i: theory and formulation. Int. J. Plast. 21, 861–882.

Chung, K., Ahn, K., Yoo, D.H., Chung, K.H., Seo, M.H., Park, S.H., 2011a. Formability of twip (twinning induced plasticity) automotive sheets. Int. J. Plast. 27, 52–81.

Chung, K., Kuwabara, T., Verma, R., 2011b. Numisheet 2011 benchmark 4: pre-strain effect on spring-back of 2d draw bending. In: Huh, H., Chung, K., Han, S.S., Chung, W.J. (Eds.), The Eighth International Conference and Workshop on Numerical Simulation of 3D Sheet Metal Forming Processes. Kaist Press, Seoul, Korea, pp. 171–175.

Eggertsen, P.A., Mattiasson, K., 2009. On the modelling of the bending-unbending behaviour for accurate springback predictions. Int. J. Mech. Sci. 51, 547–563.

Geng, L., Shen, Y., Wagoner, R., 2002. Anisotropic hardening equations derived from reverse-bend testing. Int. J. Plast. 18, 743–767.

Haddadi, H., Bouvier, S., Banu, M., Maier, C., Teodosiu, C., 2006. Towards an accurate description of the anisotropic behaviour of sheet metals under large plastic deformations: modelling, numerical analysis and identification. Int. J. Plast. 22, 2226–2271.

Hemmerich, E., Rolfe, B., Hodgson, P., Weiss, M., 2011. The effect of pre-strain on the material behaviour and the Bauschinger effect in the bending of hot rolled and aged steel. Mater. Sci. Eng.: A 528, 3302–3309.

Hu, Z., Rauch, E.F., Teodosiu, C., 1992. Work-hardening behavior of mild steel under stress reversal at large strains. Int. J. Plast. 8, 839–856.

Kim, H., Kim, C., Barlat, F., Pavlina, E., Lee, M.G., 2013. Nonlinear elastic behaviors of low and high strength steels in unloading and reloading. Mater. Sci. Eng.: A 562, 161–171.

Kuwabara, T., 2007. Advances in experiments on metal sheets and tubes in support of constitutive modeling and forming simulations. Int. J. Plast. 23, 385–419.

Lee, M.G., Kim, D., Kim, C., Wenner, M.L., Chung, K., 2005a. Spring-back evaluation of automotive sheets based on isotropic-kinematic hardening laws and non-quadratic anisotropic yield functions, part iii: applications. Int. J. Plast. 21, 915–953.

Lee, M.G., Kim, D., Kim, C., Wenner, M.L., Wagoner, R.H., Chung, K., 2005b. Spring-back evaluation of automotive sheets based on isotropic-kinematic hardening laws and non-quadratic anisotropic yield functions: part ii: characterization of material properties. Int. J. Plast. 21, 883–914.

Lee, M.G., Kim, D., Kim, C., Wenner, M., Wagoner, R., Chung, K., 2007. A practical two-surface plasticity model and its application to spring-back prediction. Int. J. Plast. 23, 1189–1212.

Lee, J.W., Lee, M.G., Barlat, F., 2012a. Finite element modeling using homogeneous anisotropic hardening and application to spring-back prediction. Int. J. Plast. 29, 13–41.

Lee, J.Y., Lee, J.W., Lee, M.G., Barlat, F., 2012b. An application of homogeneous anisotropic hardening to springback prediction in pre-strained u-draw/bending. Int. J. Solids Struct. 49, 3562–3572.

Lee, J.W., Lee, J.Y., Barlat, F., Wagoner, R., Chung, K., Lee, M.G., 2013. Extension of quasi-plastic elastic approach to incorporate complex plastic flow behavior application to springback of advanced high-strength steels. Int. J. Plast. 45, 140–159.
Morestin, F., Boivin, M., 1996. On the necessity of taking into account the variation in the young modulus with plastic strain in elastic-plastic software. Nucl. Eng. Des. 162, 107–116.
Nielsen, K., Brnnberg, N., 1993. Numisheet 1993 benchmark: simulation of the 2d draw bending process. In: Makinouchi, A., Nakamachi, E., Onate, E., Wagoner R.K. (Eds.), Proceedings of the Second International Conference NUMISHEET '93, Tokyo, Japan.
Piao, K., Lee, J., Kim, J., Kim, H., Chung, K., Barlat, F., Wagoner, R., 2012. A sheet tension/compression test for elevated temperature. Int. J. Plast. 38, 27–46.
Sun, L., Wagoner, R., 2011. Complex unloading behavior: nature of the deformation and its consistent constitutive representation. Int. J. Plast. 27, 1126–1144.
Sun, L., Wagoner, R., 2013. Proportional and non-proportional hardening behavior of dual-phase steels. Int. J. Plast. 45, 174–187.
Tang, Z.Z., Liang, J., Xiao, Z.Z., Guo, C., Hu, H., 2010. Three-dimensional digital image correlation system for deformation measurement in experimental mechanics. Opt. Eng. 49, 103601–103601-9.
Thuillier, S., Manach, P., 2009. Comparison of the work-hardening of metallic sheets using tensile and shear strain paths. Int. J. Plast. 25, 733–751.
Verma, R.K., Kuwabara, T., Chung, K., Haldar, A., 2011. Experimental evaluation and constitutive modeling of non-proportional deformation for asymmetric steels. Int. J. Plast. 27, 82–101.
Wagoner, R.H., Lim, H., Lee, M.G., 2013. Advanced issues in springback. Int. J. Plast. 45, 3–20.
Yamaguchi, K., Adachi, H., Takakura, N., 1998. Effects of plastic strain and strain path on youngs modulus of sheet metals. Met. Mater. Int. 4, 420–425.
Yin, Q., Soyarslan, C., Gner, A., Brosius, A., Tekkaya, A., 2012. A cyclic twin bridge shear test for the identification of kinematic hardening parameters. Int. J. Mech. Sci. 59, 31–43.
Yoon, J., Barlat, F., Gracio, J., Rauch, E., 2005. Anisotropic strain hardening behavior in simple shear for cube textured aluminum alloy sheets. Int. J. Plast. 21, 2426–2447.
Yoshida, F., Uemori, T., 2002. A model of large-strain cyclic plasticity describing the Bauschinger effect and workhardening stagnation. Int. J. Plast. 18, 661–686.
Yoshida, F., Urabe, M., Toropov, V., 1998. Identification of material parameters in constitutive model for sheet metals from cyclic bending tests. Int. J. Mech. Sci. 40, 237–249.
Yoshida, F., Uemori, T., Fujiwara, K., 2002. Elastic-plastic behavior of steel sheets under in-plane cyclic tension-compression at large strain. Int. J. Plast. 18, 633–659.
Yoshida, F., Urabe, M., Hino, R., Toropov, V., 2003. Inverse approach to identification of material parameters of cyclic elasto-plasticity for component layers of a bimetallic sheet. Int. J. Plast. 19, 2149–2170.
Zang, S.L., Liang, J., Guo, C., 2007. A constitutive model for spring-back prediction in which the change of young's modulus with plastic deformation is considered. Int. J. Mach. Tools Manuf. 47, 1791–1797.
Zang, S.L., Guo, C., Thuillier, S., Lee, M.G., 2011a. A model of one-surface cyclic plasticity and its application to springback prediction. Int. J. Mech. Sci. 53, 425–435.
Zang, S.L., Thuillier, S., Port, A.L., Manach, P., 2011b. Prediction of anisotropy and hardening for metallic sheets in tension, simple shear and biaxial tension. Int. J. Mech. Sci. 53, 338–347.
Zang, S.L., Lee, M.G., Kim, J.H., 2013a. Evaluating the significance of hardening behavior and unloading modulus under strain reversal in sheet springback prediction. Int. J. Mech. Sci. 77, 194–204.
Zang, S.L., Sun, L., Niu, C., 2013b. Measurements of Bauschinger effect and transient behavior of a quenched and partitioned advanced high strength steel. Mater. Sci. Eng.: A 586, 31–37.
Zhang, D., Cui, Z., Ruan, X., Li, Y., 2007. An analytical model for predicting springback and side wall curl of sheet after u-bending. Comput. Mater. Sci. 38, 707–715.
Ziegler, H., 1959. A modification of Prager's hardening rule. Q. Appl. Math. 17, 55–65.